Single-cell growth inference of *Corynebacterium glutamicum* reveals asymptotically linear growth

Joris Messelink[1,*], Fabian Meyer[3,4,*], Marc Bramkamp[3,4,+] and Chase P. Broedersz[1,2,+]

[1]*Arnold-Sommerfeld-Center for Theoretical Physics, Ludwig-Maximilians-Universität München, Theresienstrasse 37, 80333 Munich, Germany*

[2]*Department of Physics and Astronomy, Vrije Universiteit Amsterdam, 1081 HV Amsterdam, The Netherlands*

[3]*Ludwig-Maximilians-Universität München, Fakultät Biologie, Großhaderner Straße 2-4, 82152, Planegg-Martinsried, Germany*

[4] *Christian-Albrechts-Universität zu Kiel, Institut für allgemeine Mikrobiologie, Am Botanischen Garten 1-9, 24118 Kiel, Germany*

[*] These authors contributed equally

+ Corresponding authors:

Chase Broedersz

Email: c.broedersz@lmu.de, Phone: +49-(0)89- 2180-4514

Marc Bramkamp

Email: bramkamp@ifam.uni-kiel.de; Phone: +49-(0)431-8804341

Keywords| cell-size homeostasis | single-cell growth| apical growth | RodA| cell wall

Significance

Regulation of growth and cell size is crucial for the optimization of bacterial cellular function. So far, single bacterial cells have been found to grow exponentially, which implies the need for tight regulation mechanisms to maintain cell size throughout growth and division cycles. Here, we characterize the growth behavior of the apically growing bacterium *Corynebacterium glutamicum,* by developing a novel and broadly applicable inference method for single-cell growth dynamics. We find that this bacterium grows asymptotically linearly, enabling it to maintain a narrow distribution of cell sizes, despite having a large variability of single-cell growth features. Our results imply a novel interplay between mode of growth and division regulation mechanisms, which may extend to other bacteria with non-exponential growth modes.

Abstract

In many bacteria, protein mass production is thought to be rate limiting for growth, implying exponential growth at the single cell level. To maintain cell-size homeostasis in proliferating populations of exponentially growing bacteria, tight growth and division mechanisms are required. However, it remains unclear whether these considerations set universal physical limits to bacterial growth. Here, we characterize the growth dynamics of the actinobacterium *Corynebacterium glutamicum* - a promising candidate for uncovering novel growth modes. This bacterium exhibits apical cell wall synthesis and division site selection systems appear to be absent, as reflected by a broad distribution of division asymmetries. We develop a novel growth inference method that averages out measurement noise and single-cell variability to obtain elongation rate curves as a function of birth length. Using this approach, we find that *C. glutamicum* exhibits asymptotically linear single-cell growth. To explain this growth mode, we model elongation as being rate-limited by the apical growth mechanism mediated by cell wall transglycosylases. This model accurately reproduces the observed elongation rate curves, and we further validate the model with growth measurements on a transglycosylase deficient *ΔrodA* mutant. Finally, with simulations we show that asymptotically linear growth yields a narrower distribution of cell lengths, suggesting that this growth mode can act as a substitute for tight division length and division symmetry regulation.

Main Text

The principles underlying bacterial growth have been studied since the middle of the 20th century. The population level approach followed by Monod and Schaechter resulted in fundamental laws of bacterial population growth, such as the identification of population growth phases, which still provide valuable insights into the dynamics of microbial growth (1, 2). However, the growth at a single-cell level remained an open question at the time. This changed over the last decade, as evolving technologies enabled detailed measurements of growth dynamics at the single-cell level. Extensive work was done on common model organisms, including *Escherichia coli*, *Bacillus subtilis,* and *Caulobacter crescentus,* revealing that single cells grow exponentially for these species (3–7). Such exponential growth is expected if cellular volume production is proportional to the protein content (8). Importantly however, such a proportionality will only be present if cellular volume production is rate-limiting for growth. Classes of cell types with different rate-limiting steps could display distinct growth behavior, but little evidence exists for such deviations from exponential growth (9–11). Non-exponential growth modes may have important implications for growth regulatory mechanisms: while exponential growth requires checkpoints and regulatory systems to maintain a constant size distribution (4), such tight regulation might not be needed for other growth modes.

A promising candidate for uncovering novel growth modes is the Gram-positive *Corynebacterium glutamicum*. *C. glutamicum* is broadly used as a production-organism for amino-acids and vitamins and also serves as model organism for the taxonomic related human pathogens *C. diphteriae* and *Mycobacterium tuberculosis* (12–14). The cell wall of *Corynebacteria* and *Mycobacteria* is a complex polymer composed of a classical bacterial peptidoglycan (PG) sacculus that is covalently bound to an arabinogalactan (AG) layer (15). Mycolic acids are fused to the arabinose and form an outer membrane like bilayer, rendering the cell surface highly hydrophobic (16).

C. glutamicum's growth and division behavior is highly atypical. In contrast to rod-shaped firmicutes and γ-proteobacteria, where cell-wall synthesis is dependent on the lateral acting MreB, members of

the *Corynebacterianeae* lack a *mreB* homologue and elongate apically. This apical elongation is mediated by the DivIVA protein, which accumulates at the prospective new poles and serves as a scaffold for the organization of the elongasome complex (17–19) (Figure 1 A, B). Furthermore, a tightly regulated division-site selection mechanism is absent in *C. glutamicum*. Without harboring any known functional homologues of the Min- and nucleoid occlusion (Noc) system, cells partially give rise to unequal sized daughter cells (20, 21). Lastly, the spread in growth times between birth and division is much wider than in other model organisms, suggesting a weaker regulation of this growth feature (20). These atypical growth properties suggest that this bacterium is an interesting candidate to test the universality of previously reported exponential growth laws. To reveal the underlying growth regulation mechanisms, it is necessary to study the elongation dynamics of *C. glutamicum*.

Here, we combine detailed single-cell elongation measurements with a novel procedure to infer their growth behavior. Our results indicate that *C. glutamicum* deviates from the generally assumed single-cell exponential growth law. Instead, these *Corynebacteria* exhibit asymptotic linear growth. We develop a mechanistic model showing that this anomalous elongation dynamics is due to cell wall synthesis at the cell poles being the rate-limiting step for growth. Finally, we demonstrate a connection between mode of growth and the impact of single-cell variations on the cell size distribution of the population. For an asymptotically linear grower, these variations have a much smaller impact on this distribution than they would for an exponential grower, suggesting an evolutionary explanation for the lack of tight regulation of single-cell growth in *C. glutamicum.*

Results

Detailed growth trajectories are obtained from microfluidic experiments

To investigate the spatio-temporal development of single *C. glutamicum* cells, we developed a novel workflow that is not cell-type specific and includes comprehensive image-analysis, multi-dimensional descriptive statistics, and quantitative modeling. For imaging, epifluorescence microscopy was used

and cells were grown in a microfluidic device. In *C. glutamicum* the mCherry-tagged scaffold protein DivIVA provides a marker for cell cycle progression, since DivIVA localizes to the cell poles and to the newly formed division septum (17, 20).

The analysis of bacterial growth is routinely performed in microfluidic chambers. Often so-called mother machines are used (22). These devices consist of thin channels roughly matching the width of the bacteria under study and they allow for a continuous analysis of growing and dividing cells over long time periods, since new cells are pushed out of the channels and washed out with the medium flow. The bacterium *C. glutamicum* is, however, not ideally suitable for growth in traditional mother machines. A major problem is the characteristic V-snapping division that could lead to shear forces and stress during cell separation affecting growth (23). Therefore, we instead used microfluidic chambers in which cells could grow out into a 2D colony (Figure 1 A). To extract the growth dynamics from these experiments, we developed a new image analysis software to track individual cell lineages and collect high quality cell growth data without imposing external stress on the cells (Material and Methods).

Within the highly controlled environment of the microfluidic device, a steady medium feed and a constant temperature of 30 °C was maintained. The chamber architecture enabled for the cultivation of cells on a flat surface, allowing the growing colony to expand without spatial limitations into two dimensions for several generations (Figure 1 C). We extracted bright-field- and fluorescent-images within a three-minute interval, and the obtained raw-data were processed semi-automatically with a workflow developed in FIJI and R (24, 25). For each individual cell per time-frame, the data set contains the cell's length, area and estimated volume, a snapshot of the DivIVA-mCherry profile, and information about generational lineage (Figure 1 D-G). The resulting data sets were used to further investigate the growth behavior of our bacterium. Thus, using this procedure, we obtained data sets containing detailed statistics on single-cell growth.

For all subsequent growth analysis, the measured cell lengths were used. The increases in cell length are proportional to the increases in estimated cell volume (SI Figure S1 A), but are less noisy than the

latter (SI Figure S1 B). This proportionality is not unexpected since the rod-shaped *C. glutamicum* cells insert new cell wall material exclusively at the poles, while maintaining a roughly constant cell width over the cell cycle.

Population-average test shows non-exponential growth for *C. glutamicum*

A standard characterization of single-cell bacterial growth, is the average relation between the birth length l_{b} and division length l_{d} (8). For *C. glutamicum,* we find an approximately linear relationship between these two quantities, with a slope of 0.92 (Figure 2 A). This indicates that on a population level, *C. glutamicum* behaves close to the *adder* model (8, 26).

To investigate the growth dynamics from birth to division, we first tested if our cells conform to the generally observed exponential mode of single-cell growth. To this end, we applied a previously employed analysis on bacterial elongation data (27), by plotting $\ln\left(\frac{l_{\mathrm{d}}}{l_{\mathrm{b}}}\right)$ versus the growth time (Figure 2 B). For an exponential grower, with the same exponential growth rate α for all cells, the averages of $\ln\left(\frac{l_{\mathrm{d}}}{l_{\mathrm{b}}}\right)$ per growth time bin are expected to lie along a straight line with slope α that intersects the origin. By contrast, we find a systematic deviation from this trend, with cells with shorter growth times lying above this line and cells with longer growth times lying below it, suggesting non-exponential elongation behavior. However, the implications of these deviations for single-cell growth behavior are not clear from this plot. There are several quantities that could be highly variable between cells that are averaged out in this representation, such as variations in exponential growth rate as a function of initial size, or variations in growth mode over time.

The variabilities of key growth quantities cannot be easily extracted from individual growth trajectories due to measurement noise (Figure 2 C). In fact, it has been estimated that in order to distinguish between exponential and linear growth for an individual trajectory, the measurement errors in the individual length measurements have to be below ~6% (28). To distinguish more subtle growth features may require an even higher degree of accuracy.

Novel growth-inference method yields average elongation rate curves

To obtain quantitative elongation rate curves as a function of time and birth length, despite the high degree of individual variation, we developed a novel data analysis procedure that exploits the noise-reducing properties of multiple-cell conditional averaging. First, for all cells in the data set, we take the time since birth t, the cellular length L at time t and the birth length l_b Subsequently, we plot the length at time t versus birth length, yielding a scatter plot for each measurement time (Figure 3 A). For each plot, a linear fit is made through the data, yielding the average dependence of $L(t, l_\mathrm{b})$on $L(t_0, l_\mathrm{b})$ (Figure 3 B). We employ a linear fit since higher-order functions result in a negligible improvement of the goodness-of-fit, while increasing the mean error on inferred elongation rates (SI Figure S3). Note that for both purely linear and purely exponential growth, $L(t, l_\mathrm{b})$ would depend linearly on l_b: for linear growth $L(t, l_\mathrm{b}) = \alpha t + l_\mathrm{b}$, whereas for exponential growth $L(t, l_\mathrm{b}) = l_\mathrm{b}\exp(\alpha t)$ (SI Figure S5). From the fitted dependencies $L(t, l_\mathrm{b})$, we compute a series of points $\{L(t_0, l_\mathrm{b}), L(t_1, l_\mathrm{b}), L(t_2, l_\mathrm{b}), \ldots\}$, yielding the average growth trajectory of a cell starting out at length l_b. From this inference approach, we thus obtain the functional dependence of the average added length on grow time and birth length. We find the average length to steadily increase initially, but level off and show pronounced fluctuations for larger growth times (Figure 4 A, C).

This late-time behavior (dashed lines in Figure 4 A) is caused by decreasing cell numbers and a bias in the averaging procedure introduced by dividing cells (Figure 4 B). Since we infer average growth behavior, after the first division event this average would be conditioned on the cells that have not divided yet. For a given birth length, faster-growing cells divide earlier than slower-growing cells (SI Figure S2) causing this conditional average to underestimate cellular elongation rates for the whole population after the first division. Because our aim is to infer elongation curves that characterize the whole population, ranging from slow to fast growers, for further analysis only the part of each trajectory before the first division event is used. In principle, sub-population elongation curves can also be obtained that extend past the first division event, but only if the entire analysis for these curves is performed only on these slower-dividing cells (SI Figure S4).

We obtain elongation rate curves by taking a numerical derivative of smoothed growth trajectories (SI S1). To determine the associated error margins of the elongation rates, we used a bootstrapping algorithm (29). The resulting 2σ bounds are shown as semitransparent bands. Despite the high noise level of individual elongation trajectories, the inferred average elongation rates have an error margin of around 8%. Thus, our approach robustly infers average elongation trajectories from single-cell growth data. Strikingly, the elongation rate curves initially increase, but then gradually level off towards a linear growth mode (Figure 5 A and SI Figure S4). Additionally, elongation rates of cells with larger birth length are consistently higher than the elongation rates of cells with smaller birth length.

Onset of the linear growth regime does not consistently coincide with septum formation

A striking feature of the obtained elongation rate curves is a transition from an accelerating to a linear growth mode after approximately 20-25 minutes (Figure 5 A). One possibility is that this levelling off is connected with the onset of septum formation. We hypothesized, given that the FtsZ-dependent divisome propagates the invagination of the septum under the consumption of cell wall precursors (e.g. lipid-II), that the appearance of the additional sink for cell-wall building blocks could lead to coincidental leveling-off of the elongation rates (30). To test this hypothesis we imaged DivIVA-mCherry during growth, since the negative curvature of the plasma membrane, introduced by the inward growing septum, leads to the accumulation of DivIVA (31, 32). From these images, we obtained an intensity profile over the cell length, excluding the DivIVA-mCherry signal at the cell tips and averaged the intensity over the remaining area. We then marked the moment where there was a sharp increase in the average DivIVA-mCherry signal as a proxy for the moment of onset of septum formation. We observe that the moment of onset of septum formation does not consistently coincide with the moment at which the elongation rate levels off (Figure 5 A, SI Figure S6): for smaller

cells the onset of septum formation occurs much later. Therefore, it seems implausible that the observed linear growth regime is due the septum acting as a sink for cell-wall building blocks.

Polar cell wall formation is the rate-limiting step for growth, leading to a linear growth regime

To provide insight into the anomalous single-cell growth behavior, we model single-cell elongation as being rate-limited by an apical cell wall formation mechanism. To formulate this model, we first consider the biochemical pathway that leads to cell wall formation in *C. glutamicum*, as illustrated in Figure 6 A. The key process for cell wall formation in *C. glutamicum* is peptidoglycan (PG) synthesis at the cell poles, which builds the cell wall. PG intermediates are provided by the substrate lipid-II, and the integration of new material into the PG-mesh is mediated by transgylcosylases (TGs) located at the cell pole. At the TG sites, lipid-II is translocated across the plasma membrane by the lipid-II flippase MurJ (33–35). After PG building blocks provided by lipid-II are incorporated into the existing cell wall by transglycolylation, transpeptidases (TP) conduct the crosslinking of peptide subunits, which contributes to the rigidity of the cell wall (36–38). During growth, the area of the PG sacculus, and thus the number of TG sites, is extended by multiple factors recruited by DivIVA (17).

To model this growth mechanism, we assume that the rate of new cell wall formation is proportional to the number of TG sites. We describe the interaction between lipid-II and TG sites by Michaelis-Menten kinetics (Figure 6 B). Specifically, assuming the cell length added per unit time is proportional to the cell wall area added per unit time, we find

$$\frac{dL(t)}{dt} = \alpha \frac{c(t)N(t)}{K_m + c(t)} \tag{1}$$

with $L(t)$ the cell length at time t, $c(t)$ the concentration of lipid-II, K_m the Michaelis constant for this reaction, and α is a proportionality constant.

While $c(t)$ and $N(t)$ may both be time dependent in general, we first investigate simple scenarios where one of these variables is approximately constant. We immediately see that keeping $N(t)$

constant with $c(t)$ variable will not yield solutions consistent with the data: since the lipid-II concentrations should be equal directly before and directly after division, this would lead to the prediction that the elongation rates are also equal directly before and directly after division, inconsistent with our observation (Figure 5 A). By contrast, allowing $N(t)$ to be variable while keeping $c(t)$ constant yields a solution that is in accordance with the data. To derive an expression for $N(t)$, we first note that the old and new cell pole in the cell need to be treated differently. The old pole is inherited from the mother cell, and we assume the number of TG-sites at the pole to saturate within one cellular lifecycle. The new pole is assumed to initiate with the number of TG sites below saturation, and we let the number of TG sites increase proportional to the number of available sites, yielding the following kinetic description for $N(t)$:

Here, $N_{\max}$ is the maximum number of sites at the cell poles, and β is a rate constant. The solution of this differential equation is given by

$$N(t) = N_{\max} - (N_{\max} - N_0)\exp(-\beta\, t) \qquad (3)$$

with N_0 the number of TG sites at the poles at the start of growth. This result, together with Eq. (1), defines our polar growth-limited elongation model. The predicted elongation rates form a good fit to the experiment results (Figure 6 C), although the data appear to exhibit a stronger inflection.

Instead of assuming a constant recruitment of TG enzymes, we can construct a more refined model that takes TG recruitment dynamics into account. There is evidence that transglycosylase RodA and bifunctional penicillin binding proteins (PBPs) are recruited to the cell pole via the curvature-sensing protein DivIVA (17, 19). As shown in (31), DivIVA also recruits itself, leading to the exponential growth of a nucleating DivIVA cluster. Therefore, we let the recruitment rate of TG enzymes be proportional to the number of DivIVA proteins N_{D} at the pole, setting $N_{\mathrm{D}}(t) = N_{\mathrm{D}}(0)e^{\gamma t}$. This

$$\frac{dN(t)}{dt} = \beta\left(N^{\max} - N(t)\right) \qquad (2)$$

results in modified kinetic description for $N(t)$ (Eq. (2)):

$$\frac{dN(t)}{dt} = \beta\, e^{\gamma t}\left(N^{\max} - N(t)\right) \tag{4}$$

This refined model can capture more detailed features of the measured elongation rate curves (Figure 6 C), including the stronger inflection, with an additional free parameter, γ, encoding the self-recruitment rate of DivIVA.

We note that our model could be extended to allow $c(t)$ to vary with time, although this inclusion is not necessary to reproduce the observed elongation rate curves. Furthermore, if the cell is in a regime where $c(t) \gg K_m$, i.e. there is a surplus of lipid-II, the time-dependence of $c(t)$ will have little effect on the elongation rate. As the cells are grown in rich nutrient conditions, it is plausible that lipid-II synthesis is running with a high enough efficiency to operate under such saturation conditions.

The central assumption of our model is that the growth of the cell poles, mediated via accumulation of TG enzymes, is the rate-limiting step for cellular growth. To test this assumption, we repeated our experiment with a *rodA* knockout (19). The SEDS-protein RodA is a mono-functional TG (39–41). It was shown that a deletion results in a phenotype with a decreased population growth rate in the shaking-flask and a reduced average cell length (19). The cells' viability nonetheless is backed up by the presence of bifuncional class A PBPs that are capable to catalyze transglycoslyation and transpeptidation reactions. We expect this knockout to lower the efficiency of polar cell wall formation, thus slowing down the rate-limiting step of growth. Specifically, we expect the knockout of *rodA* to mainly affect the efficiency of lipid-II integration into the murein-sacculus. Within our model, this translates to a lowering of the cell wall production per transglycosylase site α. This would imply elongation rate curves of similar shape for the *ΔrodA* mutant, only scaled down by a factor $\alpha^{\mathrm{WT}}/\alpha^{\Delta\mathrm{rodA}}$. Indeed, we observe such a scaling down of the elongation rate curves (Figure 5 B), lending further credence to our model for *C. glutamicum* growth.

Birth length distribution of linear growers is more robust to single-cell growth variability

After obtaining average single-cell growth trajectories, we next asked how this growth behavior at the single cell level affects the growth of the colony. It was shown that asymmetric division and noise in individual growth times results in a dramatic widening of the cell-size distribution for a purely exponential grower (42). For an asymptotically linear grower, however, we would expect single-cell variations to have a much weaker impact.

To quantify the difference between asymptotically linear growth and hypothetical exponential growth for *C. glutamicum*, we performed population growth simulations for both cases. For the asymptotically linear growth, we assumed the elongation rate curves obtained from our model. For exponential growth, we assumed the final cell size l_{d} is given by $l_{\mathrm{d}} = l_b \exp(\alpha\, t_{\mathrm{t}} + \Delta t) + \Delta l$, with α the exponential elongation rate, t_{t} the target growth time, Δt a time-additive noise term and Δl a size-addtive noise term. All growth parameters necessary for the simulation were obtained directly from the experimental data (SI S2, SI Figure S7). From this simulation, the distribution of initial cell lengths was determined for each scenario.

The resulting distribution of birth lengths for the asymptotically linear growth case closely matches the experimentally determined distribution (Figure 7). By contrast, the distribution for exponential growth is much wider, and exhibits a broad tail for longer cell lengths. This suggests a strong connection between growth mode and the effect of individual growth variations on population statistics. *C. glutamicum* has a high degree of variation of division symmetry (SI Figure S7C) and single-cell growth times, but due to the asymptotically linear growth mode, the population-level variations in cell size are still relatively small.

Discussion

Using a novel growth trajectory inference and analysis method, we showed that *C. glutamicum* exhibits asymptotically linear growth, rather than the exponential growth generally assumed for most species. The obtained elongation rate curves are shown to be consistent with a model of apical

cell wall formation being the rate-limiting step for growth. The model is further validated by experiments with a *ΔrodA* mutant, in which the elongation rate curves look functionally similar but with a downward shift to slower rates compared to the WT case, as predicted from our model (Figure 5 B). For *C. glutamicum*, apical cell wall formation would be a plausible candidate for the rate-limiting step of growth, because synthesis of the highly complex cell wall and lipids for the mycolic acid membrane is cost intensive and a major sink for energy and carbon in *Corynebacteria* and *Mycobacteria* (43). We emphasize that our experiments were performed in rich nutrient conditions, e.g. under conditions supporting fast growth. It would be interesting to see, whether the observed mode of growth is maintained in minimal growth media.

Our proposed growth model shares similar features to recent experimental observations on polar growth in Mycobacteria (44). Polar growth was shown to follow 'new end take off' (NETO) dynamics (44), in which the new cell pole makes a transition from slow to fast growth. In our proposed growth model for *C. glutamicum*, the new pole initially increases its average elongation rate before reaching a constant maximum. However, weather a sharp 'take off' event occurs cannot be discerned from our data.

To investigate the implications of our inferred single-cell growth mode for cell-size homeostasis throughout a population of cells, we performed simulations of cellular growth and division over many generations. We found that our asymptotically linear growth model accurately reproduces the experimental distribution of cell birth lengths. By contrast, a model of exponential growth predicts a much broader distribution with a long tail for larger birth lengths. This indicates a possible connection between mode of growth and permissible growth-related noise levels for the cell. Indeed, if single-cell growth variability is reduced by a factor 3, the distributions corresponding to both growth modes show a similarly narrow width (SI Figure S8). However, an asymptotically linear grower is able to maintain a narrow distribution of cell sizes even for higher noise levels, whereas for an exponential grower this distribution widens dramatically (Figure 7).

The enhanced robustness of the length distribution of linear growers is interesting from an evolutionary point of view. Most rod shaped bacteria use sophisticated systems, such as the Min

system, to ensure cytokinesis precisely at midcell (45, 46). Bacteria encoding a Min system grow by lateral cell wall insertion. In contrast, rod-shaped bacteria in the Actinobacteria phylum such as *Mycobacterium* or *Corynebacterium* species, grow apically and do not contain a Min system, nor any other known division site selection system (21). *C. glutamicum* rather couples division site selection to nucleoid positioning after chromosome segregation via the ParAB partitioning system (20), and has a broader distribution of division symmetries. We speculate that due to *C. glutamicum's* distinct growth mechanism, a more precise division site selection mechanism was not necessary to maintain a narrow cell size distribution.

The elongation rates reported in this paper reflect the increase in cellular volume over time. However, the increase in cell *mass* is not necessarily proportional to cellular volume. In exponentially growing *E. coli,* the cellular density was recently reported to systematically vary during the cell cycle, while the surface-to-mass ratio was reported to remain constant (47). It is unknown how single-cell mass increases in *C. glutamicum*, but it would follow exponential growth if mass production is proportional to protein content. This raises the question how linear volume growth and exponential mass growth are coordinated. The presence of a regulatory mechanism for cell mass production that couples to cell volume is implied by the elongation rate curves obtained for the Δ*rodA* mutant. As the elongation rate is lower in this mutant, average mass production needs to be lowered compared to the WT in order to prevent the cellular density from increasing indefinitely.

Our growth trajectory inference method is not cell-type specific, and can be used to obtain detailed growth dynamics in a wide range of organisms. The inferred asymptotically linear growth of *C. glutamicum* is a stark deviation from the generally observed exponential single-cell bacterial growth, and suggests the presence of novel growth regulatory mechanisms.

Experimental Procedures

Strains, culture and live-cell time-lapse imaging

Exponentially growing cells of *C. glutamicum divIVA::divIVA-mCherry* and *C. glutamicum divIVA::divIVA-mCherry ΔrodA* respectively, grown in BHI–medium (Oxoid) at 30°C and 200 rpm shaking, were diluted to an OD_{600} of 0.01. According to the manufacturer's manual cells were loaded into a CellASIC- microfluidic plate type B04A (Merck Milipore) and mounted on a Delta Vision Elite microscope (GE Healthcare, Applied Precision) with a standard four-color InSightSSI module and an environmental chamber heated to 30°C. Images were taken in a three-minute interval for 10 h with a 100×/1.4 oil PSF U-Plan S-Apo objective and a DS-red-specific filter set (32% transmission, 0.025 s exposure).

Image analysis

For image analysis a custom made algorithm was developed using the open-source programs FIJI and R (24, 25). The developed workflow assigns unique identifiers to single cells, extracts the individual cell cycles from the raw image and automatically measures the parameters length, area and relative septum position from singularized cells. The documented code is available at:

https://github.com/Morpholyzer/MorpholyzerGenerationTracker

ACKNOWLEDGMENTS

This work was further funded by grants from the Deutsche Forschungsgemeinschaft (project P05in TRR174, granted to M.B. and project P06 in TRR174, granted to C.B.). J.M. is supported by a DFG fellowship within the Graduate School of Quantitative Biosciences Munich (QBM). We thank our colleagues from C.B. and M.B. groups for discussions, feedback and comments on the manuscripts.

Author contribution

J.M., F.M., M.B. and C.B. conceived the project and designed the experiments. J.M., F.M. performed theoretical and experimental parts, respectively. J.M., F.M., M.B. and C.B. analyzed the data and models and wrote the manuscript.

Figures

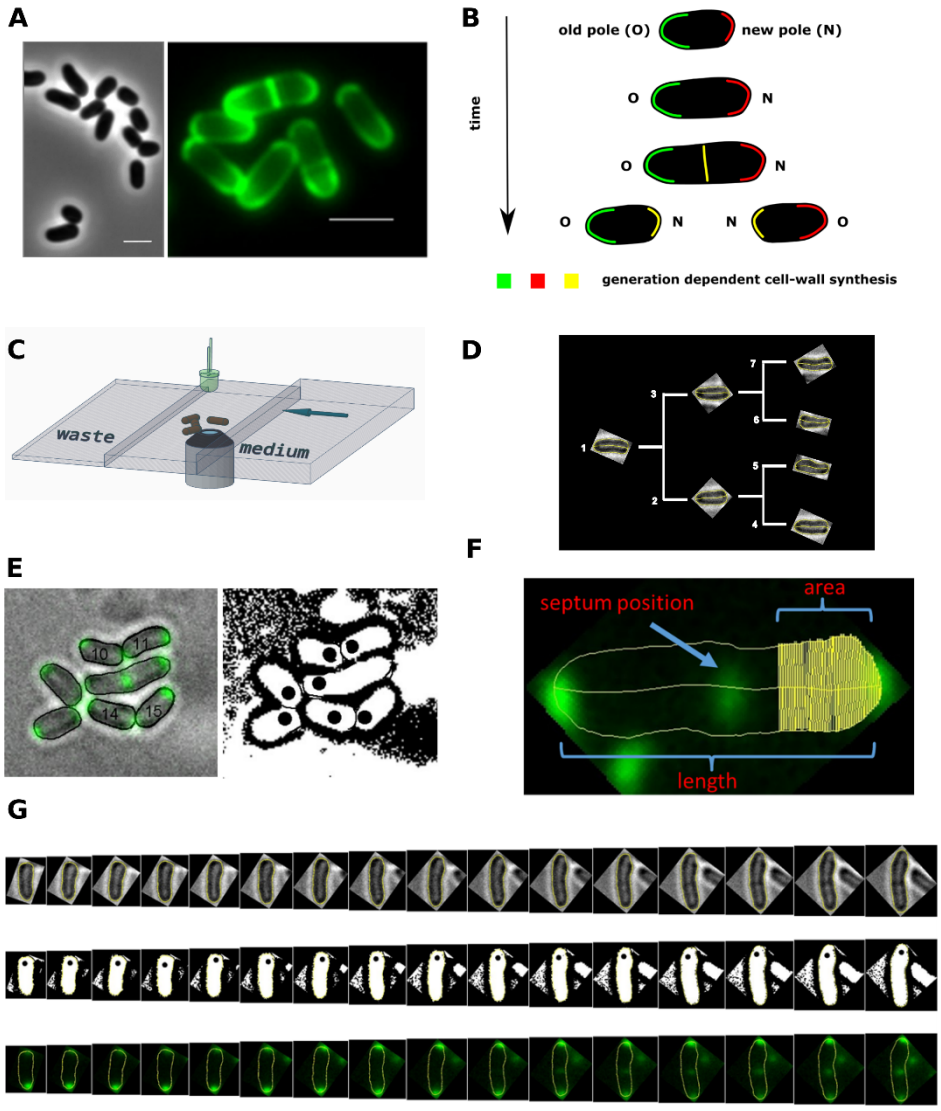

Figure 1 (A, left) Phase contrast image of *C. glutamicum* in logarithmic growth phase, indicating the variable size of daughter cells. **(A, right)** Bio-orthogonal labeling of nascent peptidoglycan (PG), indicating the asymmetric apical growth where the old cell-pole always shows a stronger activity compared to the new pole. The labeling also reveals the variable septum positioning; Bar: 2 µm **(B)** Schematic showing the generation dependent sites of PG synthesis in *C. glutamicum*, including the maturation of a new to an old cell-pole. **(C)** Illustration of the microfluidic device for monitoring of a growing colony under the microscope. **(D)** Dendrogram providing the rationale for identification of single cells in a growing colony. **(E)** Screen-shot of the developed method to extract individual cell cycles from a multi-channel time-lapse micrograph. The left panel shows a merging of the bright-field

channel and the mCherry-tagged DivIVA. The black dots in the right panel indicate the new cell pole. **(F)** Example of the developed single cell analysis algorithm, measuring the length according to the cell's geometry, as well as the cell's area and the septum position relative to the new pole. **(G)** Example of an extracted individual cell cycle from birth (left) until prior to division (right), showing the bright-field (top), the orientation (middle) and the localization of mCherry-tagged DivIVA (bottom).

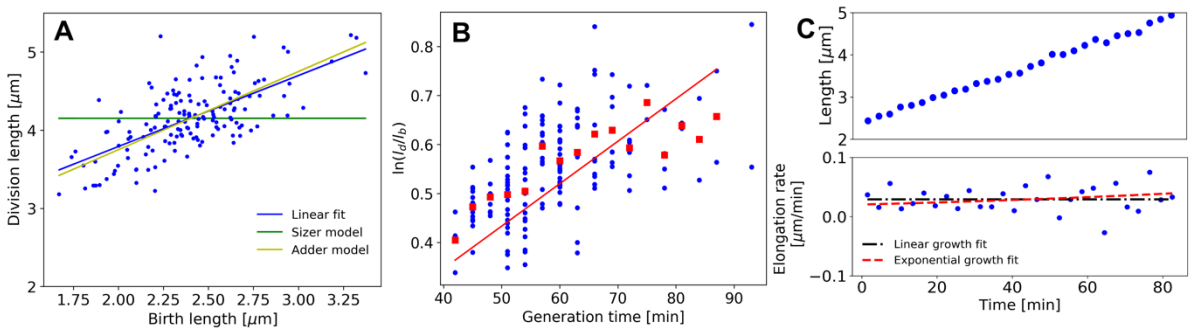

Figure 2 (A) Birth length l_b plotted against division length l_d for all measured cells, together with a linear fit (blue line), which has a slope of 0.91. Green line: best fit assuming a pure sizer (slope 0). Yellow line: best fit assuming a pure adder (slope 1). **(B)** Generation time versus $\ln\left(\frac{l_\mathrm{d}}{l_\mathrm{b}}\right)$ for all cells (blue dots) and the average per generation time (red squares). The red line represents a linear fit through the generation time averages that passes through the origin. For exponential growth, the averages would lie along this line, and the slope would be equal to the exponential growth rate. **(C)** Growth trajectory for a single cell (upper panel), together with its derivative for each measurement interval (lower panel). Fits to the derivative are shown for linear growth (black dash-dotted line) and exponential growth (red dashed line).

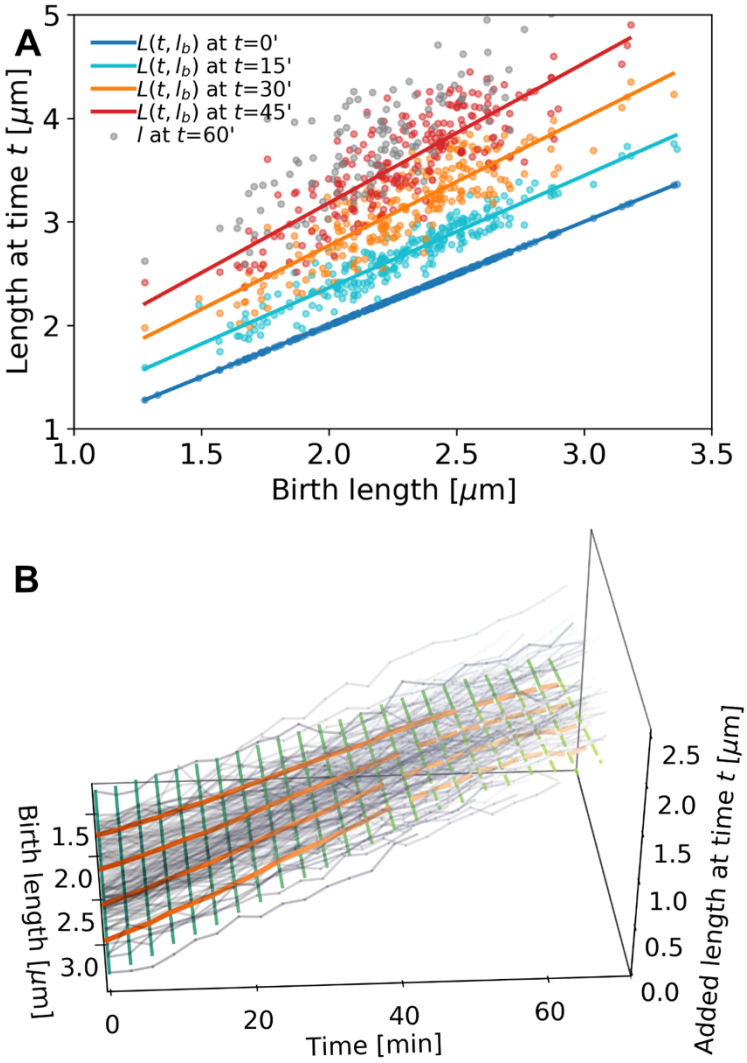

Figure 3 (A) For each cell, the length $L(t)$ at different times t since birth is plotted as a function of birth length l_b. A linear fit of the resulting "wave front" is performed for each time t. This allows us to determine average cell length $L(t, l_b)$ at time t as a function of birth length l_b. **(B)** 3D representation of the inference method of average length trajectories, with the added length $L(t, l_b) - l_b$ on the z-axis. Elongation trajectories for individual cells are indicated in grey, linear fits through all cell lengths at each timestamp are indicated by green lines. The orange lines represent four sample average length trajectories, obtained by connecting all values of the green lines associated with one birth length. Dotted lines represent regimes where averages are biased due to dividing cells.

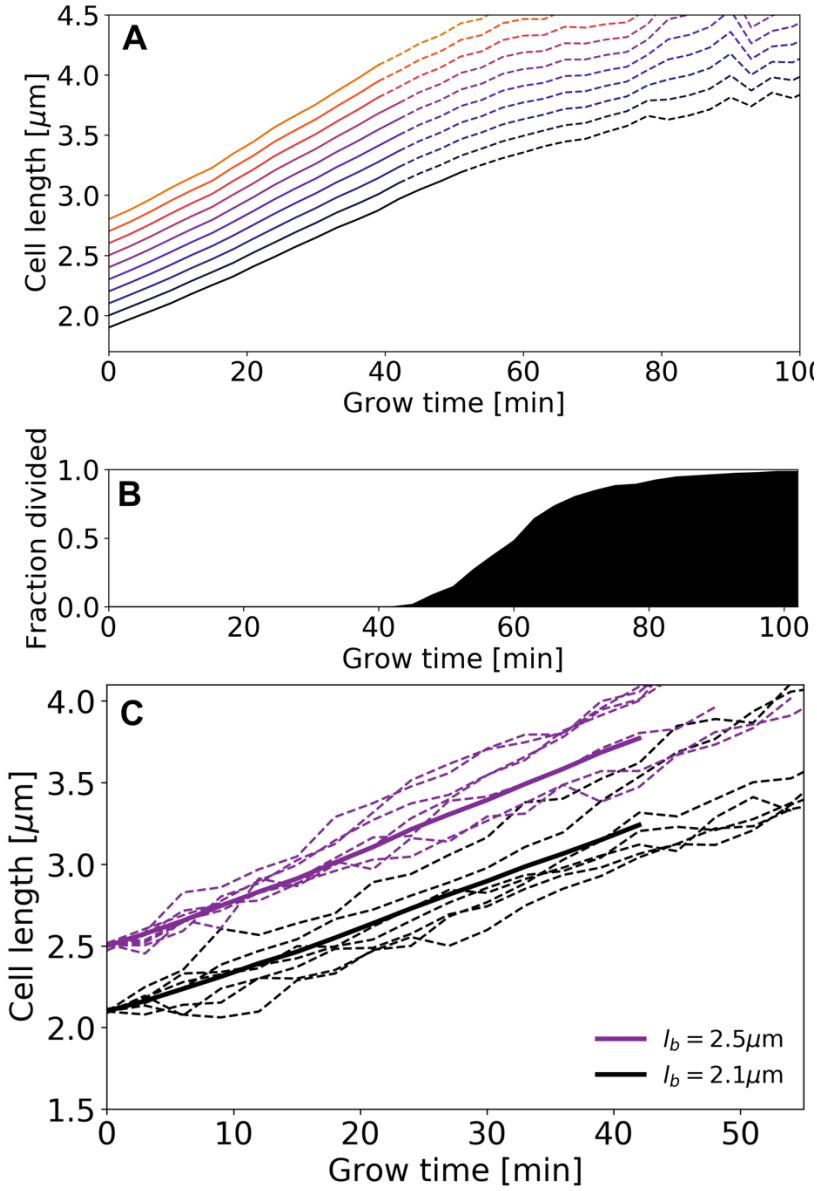

Figure 4 (A) Average elongation trajectories obtained from the fits shown in Fig. 3A for a range of birth lengths, starting at 1.9 μm with steps of 0.1μm (solid lines). The dashed lines represent regions where the inferred elongation curves are biased due to dividing cells, and are excluded from subsequent analysis. **(B)** Cumulative fraction of cells divided as a function of grow time. **(C)** Elongation trajectories for cells with birth lengths close to 2.5 μm (purple dashed lines) and birth lengths close to 2.1 μm (black dashed lines) together with their respective inferred average trajectories (purple solid line and black solid line).

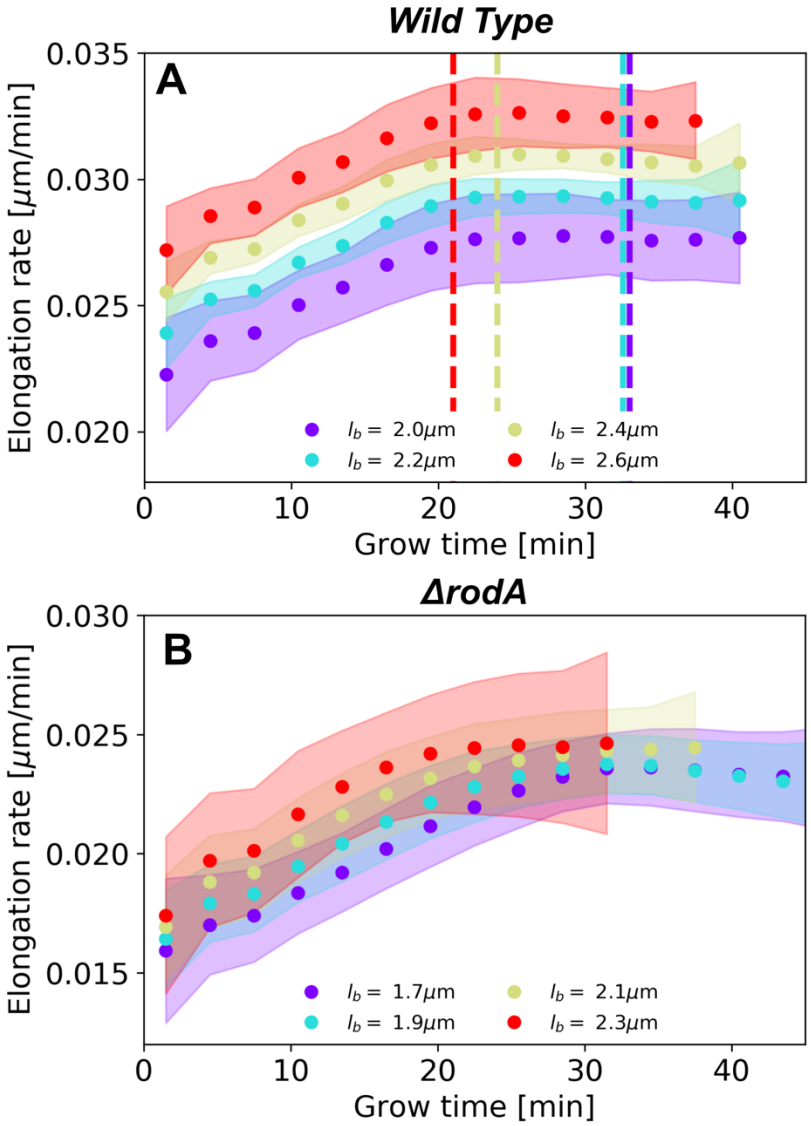

Figure 5 (A) Inferred average elongation rate trajectories for four birth lengths (dots). The 2σ confidence intervals obtained by bootstrapping are indicated by the shaded areas. Vertical dashed lines: average onset of septum formation per birth length. **(B)** Average elongation rate trajectories for the *ΔrodA* mutant.

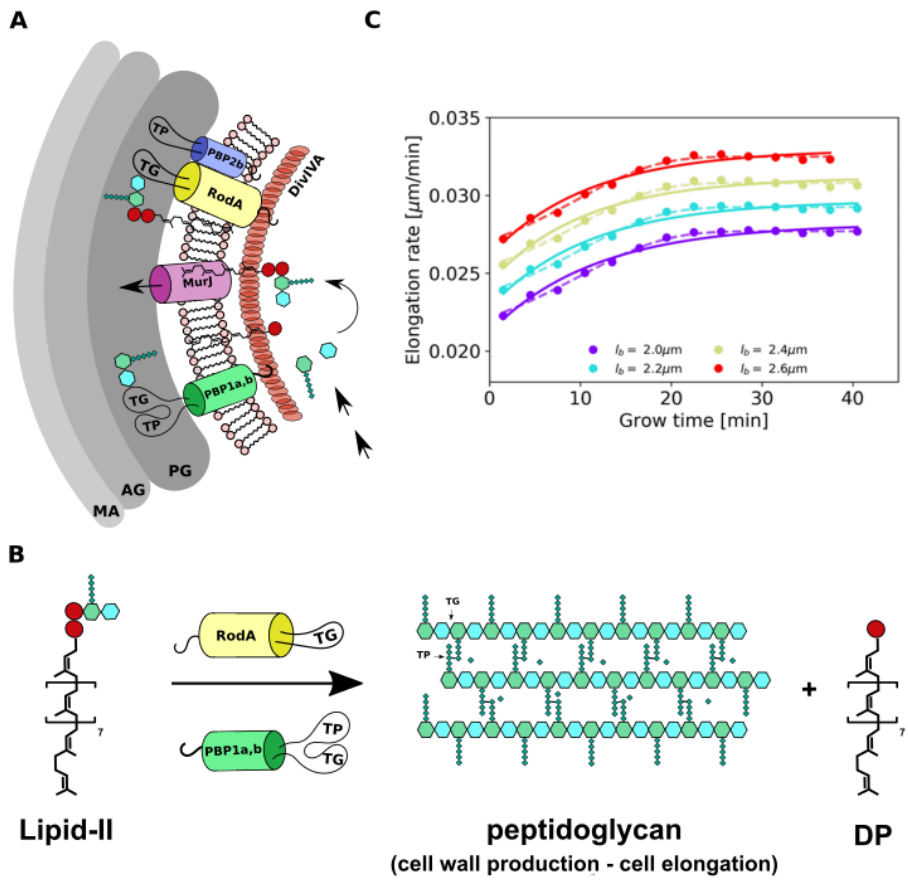

Figure 6 (A) Simplified model of the elongasome architecture of *C. gluatmicum*. The protein DivIVA serves as a scaffold at the curved membrane of the cell-pole for the recruitment of the Lipid-II flippase MurJ and several mono- and bi-functional trans-peptidases (TP) and -gylcosylases (TG). In the process of elongation, peptidoglycan (PG) precursors are integrated into the existing PG sacculus, which serves as a scaffold of the synthesis of the arabinogalactan-layer (AG) and the mycolic-acid bilayer (MA). **(B)** To model the proposed elongation mechanism, we identified two components of apical growth as the most likely rate-determining factors: the concentration of lipid-II and the number of TG sites. The corresponding Michaelis-Menten equation describes the change of length over time as function of the lipid-II concentration ($c(t)$) and the number of the TG sites ($N(t)$). **(C)** Dots: average elongation rate curves as shown in Figure 5A. Solid lines: best fit of elongation model from Eq. (3), which assumes constant transglycosylase recruitment. Dashed lines: best fit of elongation model from Eq. (4), which assumes an exponential increase of transglycosylase recruitment.

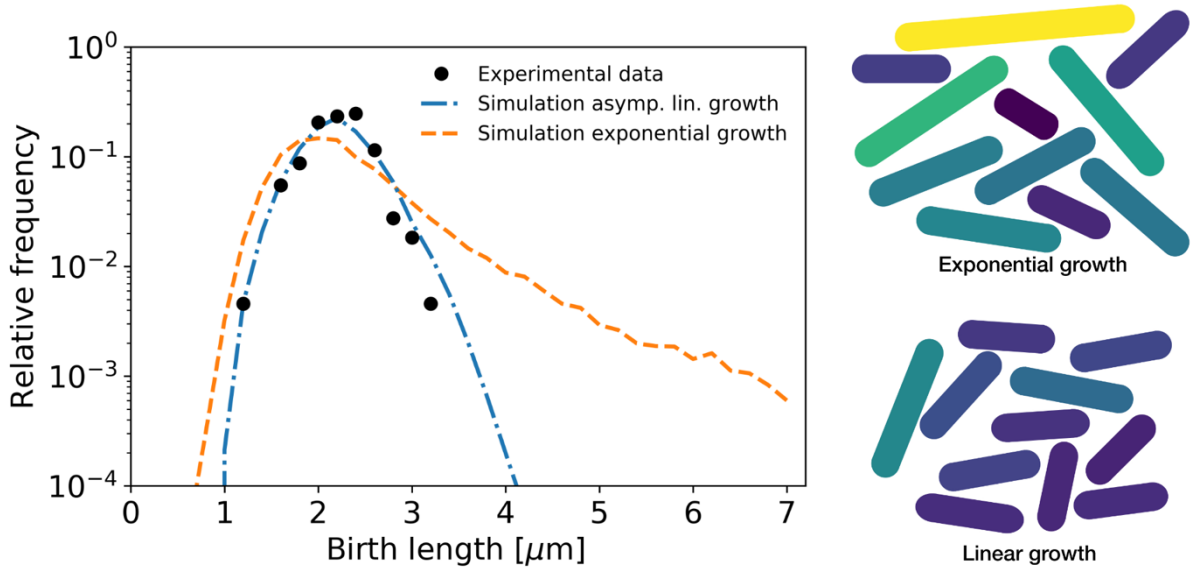

Figure 7 Birth length distribution for simulated asymptotically linear growth (blue dash-dotted line), and for simulated exponential growth (orange dashed line). For both simulations, all relevant growth parameters and distributions are obtained directly from the experimental data. Black dots: experimental birth length distribution. Right: sample of 11 cells from the exponential and asymptotically linear growth simulations, color coded according to length.

References

1. Monod J (1949) The growth of bacterial cultures. *Annu Rev Microbiol* 3:371–394.
2. Schaechter M, Maaløe O, Kjeldgaard NO (1958) Dependency on medium and temperature of cell size and chemical composition during balanced growth of *Salmonella typhimurium*. *J Gen Microbiol* 19(3):592–606.
3. Taheri-Araghi S, *et al.* (2015) Cell-size control and homeostasis in bacteria. *Curr Biol* 25:385–391.
4. Mir M, *et al.* (2011) Optical measurement of cycle-dependent cell growth. *Proc Natl Acad Sci* 108:13124–13129.
5. Iyer-Biswas S, *et al.* (2014) Scaling laws governing stochastic growth and division of single bacterial cells. *Proc Natl Acad Sci* 111:15912–15917.
6. Yu FB, *et al.* (2017) Long-term microfluidic tracking of coccoid cyanobacterial cells reveals robust control of division timing. *BMC Biol* 15:1–14.
7. Godin M, *et al.* (2010) Using buoyant mass to measure the growth of single cells. *Nat Methods* 7:387–390.
8. Amir A (2014) Cell Size Regulation in Bacteria. *Phys Rev Lett* 112:208102.
9. Aldridge BB, *et al.* (2012) Asymmetry and aging of mycobacterial cells lead to variable growth and antibiotic susceptibility. *Science* 335(6064):100–104.
10. Santi I, Dhar N, Bousbaine D, Wakamoto Y, McKinney JD (2013) Single-cell dynamics of the chromosome replication and cell division cycles in *mycobacteria*. *Nat Commun* 4:3–8.
11. Priestman M, Thomas P, Robertson BD, Shahrezaei V (2017) *Mycobacteria* modify their cell size control under sub-optimal carbon sources. *Front Cell Dev Biol* 5:64.
12. Antoine I, Coene M, Cocito C (1988) Size and homology of the genomes of leprosy-derived *corynebacteria*, *Mycobacterium leprae*, and other *corynebacteria* and *mycobacteria*. *J Med Microbiol* 27:45–50.
13. Hermann T (2003) Industrial production of amino acids by coryneform bacteria. *J Biotechnol* 104:155–172.
14. Schubert K, *et al.* (2017) The antituberculosis drug ethambutol selectively blocks apical growth in CMN group bacteria. *MBio* 8:1–21.
15. Alderwick LJ, Harrison J, Lloyd GS, Birch HL (2015) The *mycobacterial* cell wall - peptidoglycan and arabinogalactan. *Cold Spring Harb Perspect Med* 5(8):a021113.
16. Puech V, *et al.* (2001) Structure of the cell envelope of *corynebacteria*: Importance of the non-covalently bound lipids in the formation of the cell wall permeability barrier and fracture plane. *Microbiology* 147:1365–1382.
17. Letek M, *et al.* (2008) DivIVA is required for polar growth in the MreB-lacking rod-shaped actinomycete *Corynebacterium glutamicum*. *J Bacteriol* 190:3283–3292.
18. Hett EC, Rubin EJ (2008) Bacterial growth and cell division: a mycobacterial perspective. *Microbiol Mol Biol Rev* 72:126–156.
19. Sieger B, Schubert K, Donovan C, Bramkamp M (2013) The lipid II flippase RodA determines morphology and growth in *Corynebacterium glutamicum*. *Mol Microbiol* 90:966–982.

20. Donovan C, Schauss A, Krämer R, Bramkamp M (2013) Chromosome segregation impacts on cell growth and division site selection in *Corynebacterium glutamicum*. *PLoS One* 8(2).

21. Donovan C, Bramkamp M (2014) Cell division in *corynebacterineae*. *Front Microbiol* 5:132.

22. Long Z, *et al.* (2013) Microfluidic chemostat for measuring single cell dynamics in bacteria. *Lab Chip* 13:947–954.

23. Bertozzi CR, *et al.* (2019) Sequential assembly of the septal cell envelope prior to V snapping in *Corynebacterium glutamicum*. *Nat Chem Biol* 15:221–231.

24. Schindelin J, *et al.* (2012) Fiji: an open-source platform for biological-image analysis. *Nat Methods* 9:676–682.

25. R Development Core Team (2003) R: A language and environment for statistical computing.

26. Jun S, Taheri-Araghi S (2015) Cell-size maintenance: universal strategy revealed. *Trends Microbiol* 23:4–6.

27. Logsdon MM, *et al.* (2017) A parallel adder coordinates mycobacterial cell-cycle progression and cell-size homeostasis in the context of asymmetric growth and organization. *Curr Biol* 27:3367-3374.e7.

28. Cooper S (2006) Distinguishing between linear and exponential cell growth during the division cycle: Single-cell studies, cell-culture studies, and the object of cell-cycle research. *Theor Biol Med Model* 3:10.

29. Efron B (1979) Bootstrap Methods: Another look at the jackknife. *Ann Stat* 7:1–26.

30. Scheffers DJ, Tol MB (2015) LipidII: Just another brick in the wall? *PLoS Pathog* 11:1–12.

31. Lenarcic R, *et al.* (2009) Localisation of DivIVA by targeting to negatively curved membranes. *EMBO J* 28:2272–2282.

32. Strahl H, Hamoen LW (2012) Finding the corners in a cell. *Curr Opin Microbiol* 15:731–736.

33. Sham LT, *et al.* (2014) MurJ is the flippase of lipid-linked precursors for peptidoglycan biogenesis. *Science* 345(6193):220–222.

34. Kuk ACY, Mashalidis EH, Lee SY (2017) Crystal structure of the MOP flippase MurJ in an inward-facing conformation. *Nat Struct Mol Biol* 24:171–176.

35. Butler EK, Davis RM, Bari V, Nicholson PA, Ruiz N (2013) Structure-function analysis of MurJ reveals a solvent-exposed cavity containing residues essential for peptidoglycan biogenesis in *Escherichia coli*. *J Bacteriol* 195:4639–4649.

36. Scheffers DJ, Pinho MG (2005) Bacterial cell wall synthesis: New insights from localization studies. *Microbiol Mol Biol Rev* 69:585–607.

37. Valbuena V, *et al.* (2007) Characterization of HMW-PBPs from the rod-shaped actinomycete *Corynebacterium glutamicum*: Peptidoglycan synthesis in cells lacking actin-like cytoskeletal structures. *Mol Microbiol* 66:643–657.

38. Schleifer KH, Kandler O (1972) Peptidoglycan types of bacterial cell walls and their taxonomic implications. *Bacteriol Rev* 36:407–477.

39. Meeske AJ, *et al.* (2016) SEDS proteins are a widespread family of bacterial cell wall polymerases. *Nature* 537:634–638.

40. Emami K, *et al.* (2017) RodA as the missing glycosyltransferase in *Bacillus subtilis* and antibiotic discovery for the peptidoglycan polymerase pathway. *Nat Microbiol* 2:16253.

41. Sjodt M, *et al.* (2018) Structure of the peptidoglycan polymerase RodA resolved by evolutionary coupling analysis. *Nature* 556:118–121.

42. Marantan A, Amir A (2016) Stochastic modeling of cell growth with symmetric or asymmetric division. *Phys Rev E* 94:1–18.

43. Brennan PJ (2003) Structure, function, and biogenesis of the cell wall of *Mycobacterium tuberculosis*. *Tuberculosis* 83:91–97.

44. Hannebelle MTM, *et al.* (2020) A biphasic growth model for cell pole elongation in *mycobacteria*. *Nat Commun* 11(1):1-10.

45. Bramkamp M, Baarle S (2009) Division site selection in rod-shaped bacteria. *Curr Opin Microbiol* 12:683–688.

46. Lutkenhaus J (2007) Assembly dynamics of the bacterial MinCDE system and spatial regulation of the Z ring. *Annu Rev Biochem* 76:539–562.

47. Oldewurtel ER, Kitahara Y, Cordier B, Özbaykal G, Teeffelen S (2019) Bacteria control cell volume by coupling cell-surface expansion to dry-mass growth. *bioRxiv* 769786.